Volcanology and magma geochemistry of the present day activity: constraints on the feeding system

Volcanology and Magma Geochemistry of the Present-Day Activity: Constraints on the Feeding System

Antonella Bertagnini,[1] Nicole Métrich,[1,2] Lorella Francalanci,[3] Patrizia Landi,[1] Simone Tommasini,[3] and Sandro Conticelli[3]

Stromboli volcano is famous in the scientific literature for its persistent state of activity, which began about 1500 years ago and consists of continuous degassing and mild intermittent explosions (normal Strombolian activity). Rare lava emissions and sporadic more violent explosive episodes (paroxysms) also occur. Since its formation, the present-day activity has been dominated by the emission of two basaltic magmas, differing chiefly in their crystal and volatile contents, whose characteristics have remained constant until now. The normal Strombolian activity and lava effusions are fed by a crystal-rich, degassed magma, stored within the uppermost part of the plumbing system, whereas highly vesicular, crystal-poor light-colored pumices are produced during paroxysms testifying to the ascent of volatile-rich magma batches from deeper portions of the magmatic system. Mineralogical, geochemical, and isotopic data, together with data on the volatile contents of magmas, are presented here with the aim of discussing (1) the relationships between the different magma batches erupted at Stromboli, (2) the mechanisms of their crystallization and transfer, (3) the plumbing system and triggering mechanisms of Strombolian eruptions.

1. INTRODUCTION

For a long time, the volcanic island of Stromboli in the Aeolian arc (Southern Italy) has been attracting scientists and travelers because of its persistent state of mild explosive activity, usually visible for several kilometers.

[1]Istituto Nazionale di Geofisica e Vulcanologia, Sezione di Pisa, Pisa, Italy.

[2]Laboratoire Pierre Süe, CEA-CNRS, CE-Saclay, Gif/Yvette, France.

[3]Dipartimento di Scienze della Terra, Università degli Studi di Firenze, Firenze, Italy.

The Stromboli Volcano: An Integrated Study of the 2002–2003 Eruption
Geophysical Monograph Series 182

10.1029/182GM04

The subaerial part of the volcano was built in the last 100 ka, through six main periods of effusive and explosive activity (Paleostromboli I, II, and III, Vancori, Neostromboli, and Recent Stromboli; *Hornig-Kjarsgaard et al.* [1993]). Transitions between each period are marked by significant structural modifications of the edifice (caldera collapses during the early evolution and sector collapses after the Vancori period [*Tibaldi et al.*, this volume] and by significant changes in the magma composition from calc-alkaline to shoshonitic, through high-K calc-alkaline [*Francalanci et al.*, 1988, 1989; *Horning-Kjarsgaard et al.*, 1993].

The activity of the volcano, its eruptive features, its recurrent eruptive phenomena, and the morphological evolution of the crater area have been widely described in reports and scientific works since the end of the 17th century [*Barberi et al.*, 1993 and references therein]. The oldest unequivocal account of the Stromboli activity dates back to the 10th century A.D., whereas the earlier, rare historical sources are from the 4th century B.C. These historical records, however, do not

allow the exact recognition of the beginning of the persistent state of activity [*Rosi et al.*, 2000 and references therein].

Chronostratigraphic studies suggested that the present-day eruptive behavior began after a period of dormancy, nearly 1500 years ago and since then has continued without significant breaks or changes in eruptive style [*Rosi et al.*, 2000].

In the previous centuries, at least until the 4th century B.C., activity was dominated by repeated episodes of sustained fire fountains, separated by either quiescence or periods of mild Strombolian activity. In this time span, lava effusions also occurred from an adventive vent, on the northeastern flank of the volcano, pouring out the San Bartolo lava flow, which is dated between 360 B.C. and 100 A.D. by paleomagnetic and archeomagnetic methods [*Speranza et al.*, 2008; *Arrighi et al.*, 2004] (Figure 1). Magmas feeding this period of activity were fairly porphyritic (20–25 vol % of phenocrysts) high-K (HK) basaltic andesites [*Rosi et al.*, 2000; *Petrone et al.*, 2006].

The present-day activity takes place at three main craters located in a flattish area (the Crater Terrace) at 750 m above sea level (asl) within the Sciara del Fuoco (SdF), a deep horseshoe scar in the NW sector of the island, likely resulting from at least four sector collapses [*Tibaldi et al.*, this volume] (Figure 1). Since the early observations, the position of active craters has remained almost unchanged, whereas their morphology has been repeatedly modified [*Washington*, 1917]. As an example, pictures of the Crater Terrace taken in a time interval of 2 years are shown in Figure 2.

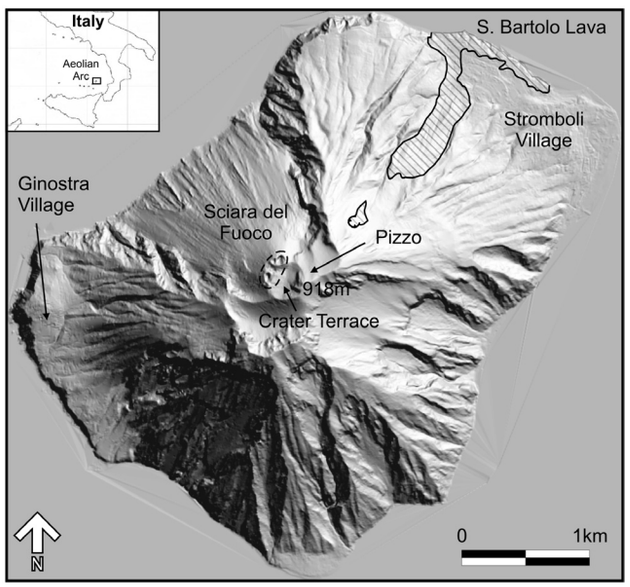

Figure 1. Map of the island of Stromboli. The position of San Bartolo lava is from *Hornig-Kjarsgaard et al.* [1993].

The persistent activity consists of continuous streaming of gas from the crater area [*Allard et al.*, 1994; this volume], mild intermittent explosions (normal Strombolian activity), rare lava emissions and sporadic more violent explosive episodes (paroxysms) [*Barberi et al.*, 1993]. Normal Strombolian activity and lava flows do not represent seriously hazardous phenomena. On the contrary, paroxysms due to their violent character and sudden occurrence are a major threat to people either visiting the volcano summit or living in the settled areas. In the last two centuries, large-scale paroxysms have produced damage to the villages of Stromboli and Ginostra, located along the coast at distances of 2–3 km from the craters.

Volcanological studies highlighted that normal Strombolian activity is characterized by the emission of highly porphyritic black scoriae (hereafter HP scoria or HP magma). In contrast, the paroxysms recorded in the last century and previous large-scale paroxysms (hereafter the historical paroxysms) produced low porphyritic golden pumices (hereafter LP pumice or LP magma) in addition to black HP scoriae identical to those of the normal Strombolian activity.

In this paper, we present a review of the most recent data with the aim of elucidating the main volcanological characteristics of the present-day activity; chemical, isotopic, and mineralogical data together with those regarding the volatile content of magmas. They are used to discuss the petrological evolution of the volcanic systems and put constraints on the Stromboli plumbing system(s).

2. VOLCANOLOGICAL CHARACTERISTICS OF THE PRESENT-DAY ACTIVITY

2.1. Normal Strombolian Activity

Normal activity consists of rhythmic, mild to moderate events lasting a few seconds, which take place at different vents every 10–20 min, and eject gas, scoriae, ash, bombs, and blocks that are thrown up to heights of several hundred meters. The proportion between different types of ejecta is variable with a prevalence of coarse ballistic ejecta or ash-charged plumes or both [*Chouet et al.*, 1999; *Patrick et al.*, 2007]. The fallout of the coarsest ejecta is usually limited to a few hundred meters from the source vent. Typical products of the normal activity are highly porphyritic (HP) black scoriae and spatter clasts. Vesicle number and texture are variable in scoria reflecting different intensity and style of the Strombolian explosions and/or a different melt rheology in the shallow conduit [*Lautze and Houghton*, 2005, 2007; *Burton et al.*, 2007b] (Plates 1a and 1b).

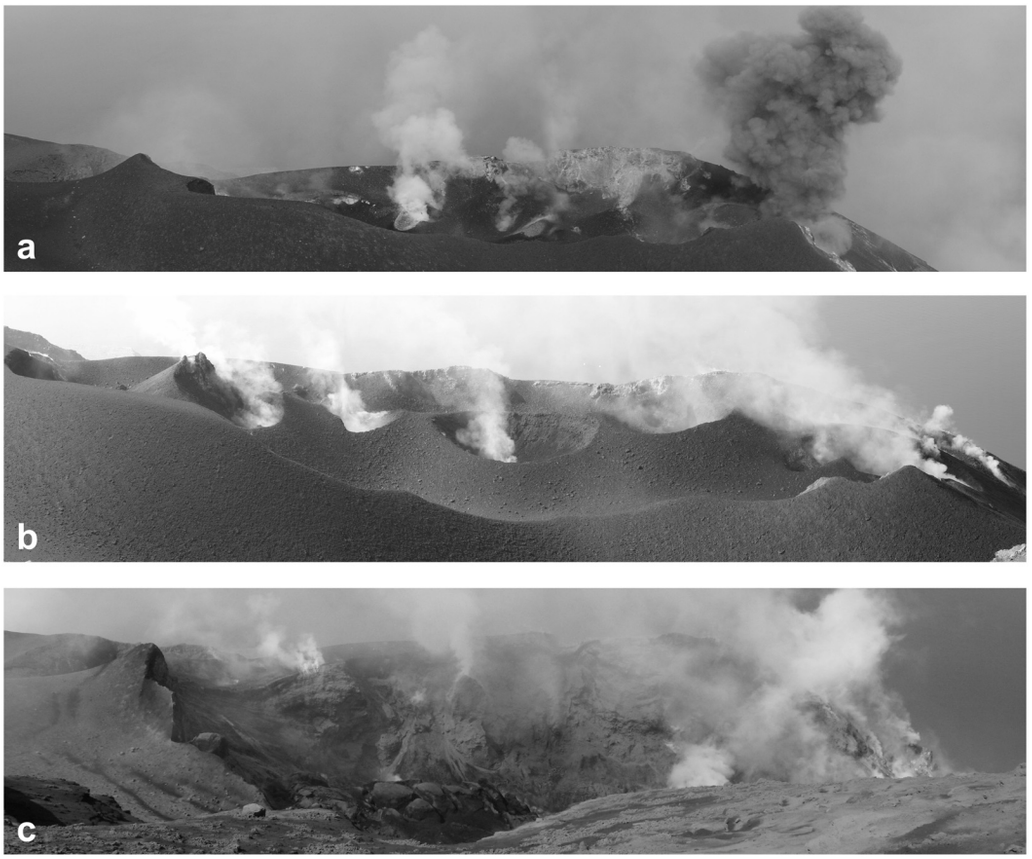

Figure 2. The Crater Terrace seen from Pizzo; (a) 2 June 2005; (b) 1 October 2006; (c) 11 April 2007.

2.2. Lava Flow Emission

Lava flows are usually produced by overflows from the summit craters or by vents opened inside the SdF, a few hundred meters below the Crater Terrace. The opening of a vent at shoreline level was reported to have occurred in 1955 [*Abbruzzese and Cavallaro*, 1956]. No evidence of vent opening outside the SdF exists in the present period of activity. Twenty-six episodes of lava emission occurred between 1888 and 2002, with duration varying from some days to 11 months. The last significant lava effusion preceding the 2002–2003 crisis lasted 141 d (from December 1985 to April 1986) and produced a lava volume of $5–6 \times 10^6$ m^3 [*De Fino et al.*, 1988]. Two small overflows from the summit craters occurred in May 1993 during a period of vigorous Strombolian activity [*Bonaccorso et al.*, 1996]. During the lava emission, Strombolian activity at the central craters is usually reported. Only scarce information is available on the state of the activity in the period preceding effusive episodes. A significant rising of the magma level in the conduits was reported 15–20 d before the beginning of the 1915 lava effusion that lasted 6 months [*Perret*, 1916]. Lava flows associated with paroxysms are also reported (see below). A short explosive phase was reported at the beginning of the 1954, 1975, and 1985 effusive episodes [*Nappi*, 1976; *De Fino et al.*, 1988]. Magma emitted during lava flow activity is a crystal-rich magma, identical to that commonly sustaining normal Strombolian activity.

2.3. Paroxysms

More energetic explosive episodes, so called Strombolian paroxysms [*Mercalli*, 1907] occur sporadically.

They usually consist of a sequence of explosive events from different craters (Plate 2a) lasting from a few minutes to days, even weeks as reported in November 1882 [*Mercalli*, 1884] and April 1907 [*Platania*, 1910]. Strong detonations, described by eyewitnesses as single or repeated cannon shots, and window-breaking pressure waves [*Riccò and Mercalli*, 1892; *De Fiore*, 1923] are accompanied by the

impulsive emission of hundred-meters-high jets of gas, ash, and incandescent materials rapidly evolving into convective plumes, up to 10 km high [*Barberi et al.*, 1993]. *Barberi et al.* [1993] classified the explosive events more energetic than those of the normal Strombolian activity on the basis of their hazard implications: "paroxysms" being the events affecting the settled areas and "major explosions" only the upper part of the volcano. However, a real limit in terms of intensity and magnitude does not correspond to these two categories. For this reason, hereafter, we refer to these episodes with the general term of "paroxysms."

During small-scale paroxysms, decimeter-sized ballistic blocks and bombs are ejected within a distance of several hundred meters from the Crater Terrace. Ash and scattered light-lapilli fallout are restricted to the volcano slopes as what typically occurred in August 1998 or August 1999 (Plate 2b). During the paroxysm of 11 July 1959, which can be considered as an intermediate-scale event, the fallout of ash, lapilli, and scattered juvenile bombs on the volcano slopes was more intense (Plate 2d), and the proximal pumice deposit reached a thickness of 40–60 cm [*Cavallaro*, 1962]. During the large-scale paroxysms, meter-sized clasts fall on the volcano slopes up to a few kilometers (Plate 2c). Heavy rain of meter-sized spatter clasts, decimeter-sized bombs, lapilli, and ash covers the volcano as described in 1930 [*Rittmann*, 1931]. Likewise, red ash covering the sea, floating pumice for several miles around the island and "pumice banks" were reported during large-scale paroxysms of the 19th century [*Mercalli*, 1881, 1883, 1884]. Lapilli fallout issued from the large-scale events led to the accumulation of alternating discrete layers of pumice and ash on the downwind slopes up to low elevations. They are usually associated with incipiently welded deposits mainly formed by decimeter-sized fluidal spatter clasts cropping out on the SdF flanks down to elevations of about 200 m asl. In some cases, the rapid accumulation of incandescent clasts on the upper sandy slopes triggered hot avalanches that reached the sea (1930, 1944).

Tsunami waves also occurred in association with some past paroxysms such as in 1879, 1916, 1919, 1930, 1944, and 1954 [*Mercalli*, 1881; *Rittmann*, 1931; *Maramai et al.*, 2005]. According to eyewitnesses' accounts, *Maramai et al.* [2005] suggested that most of these events could be related to submarine failure of the SdF. Paroxysms produced also deep changes in the crater area as in 1930 when the crater terrace lowered by about 70 m [*Rittmann*, 1931] or in 1936 when a large collapse crater formed [*Abbruzzese*, 1937].

The volume of products is always low. A rough estimate of the volume of the juvenile component gives maximum values of 10^3–10^5 m^3. The total volume of the emitted products, both juvenile and lithic clasts, is probably less than 10^6 m^3 in the largest events [*Bertagnini et al.*, 2003].

The reported state of the volcano before paroxysmal episodes is highly variable. No variations in the normal state of activity were reported before the 1930 and 1936 large-scale paroxysms, February 1993, February and October 1996 small-scale paroxysms. In contrast, the explosive activity increased for days and months before the paroxysms of 1907, 1912, 1916, 1919, 1959; overflows or lava flows occurred immediately before and during the paroxysmal crisis of 1916, 1919, 1930, 1936, and 1941. Two paroxysms took place during a 6-month-long effusive crisis with lava flows inside the SdF and mild explosive activity at the craters in 1915 [*Platania*, 1910; *Riccò*, 1917; *De Fiore*, 1915, 1923; *Ponte*, 1919, 1921; *Rittmann*, 1931; *Abbruzzese*, 1937; *Ponte*, 1948; *Cavallaro*, 1957, 1962; *Bonaccorso et al.*, 1996; *Coltelli et al.*, 2000]. The last two paroxysms (5 April 2003 and 15 March 2007) occurred during effusive episodes, after 3 months (in the 2003 event) and 15 d (in the 2007 event, see http://www.ct.ingv.it/) of intense lava effusion.

In the last 15 years, about 24 well-documented paroxysms were reported [*Barberi et al.*, 1993; *Bonaccorso et al.*, 1996; *Coltelli et al.*, 2000; http://www.ct.ingv.it/; http://www.volcano.si.edu/]. They can be classified as small-scale events except the last episodes in 5 April 2003 and 15 March 2007. It is necessary to go back about 50 years, in 1959, to find a similar event. However, they are less energetic than the 1930-type paroxysm. According to *Barberi et al.* [1993], in the last two centuries, about 25 large-scale paroxysms occurred, but assessing their number and frequency from the beginning of the present-day activity is not an easy task.

Recent paleomagnetic data on lava spatter deposits cropping out along the SdF rims suggest that the largest, spatter-forming paroxysms occurred in two distinct clusters, respectively, between 1400 and 1600 A.D. and in the 20th century [*Speranza et al.*, 2004]. *Arrighi et al.* [2004], by using archeomagnetic method, date spatter deposits cropping out on the northern flank of the volcano to the 20th century and point out the occurrence of a large paroxysmal eruption in 550 AD (±50), possibly related to the beginning of the present activity.

The unquestionable signature of Strombolian paroxysms is the production of highly vesicular, crystal-poor, light-colored ("golden") pumices. These are variably expanded and show various textures (Plate 1). Pumices result from the eruption of LP magma, wrapping HP scoria lamps and even mingled with the HP magma feeding the normal Strombolian activity and lava flows. The extent of mingling is highly variable among clasts issued from one single event and from different paroxysms (Plate 1). Unmingled HP products, identical to those emitted by the normal Strombolian activity, are present as well.

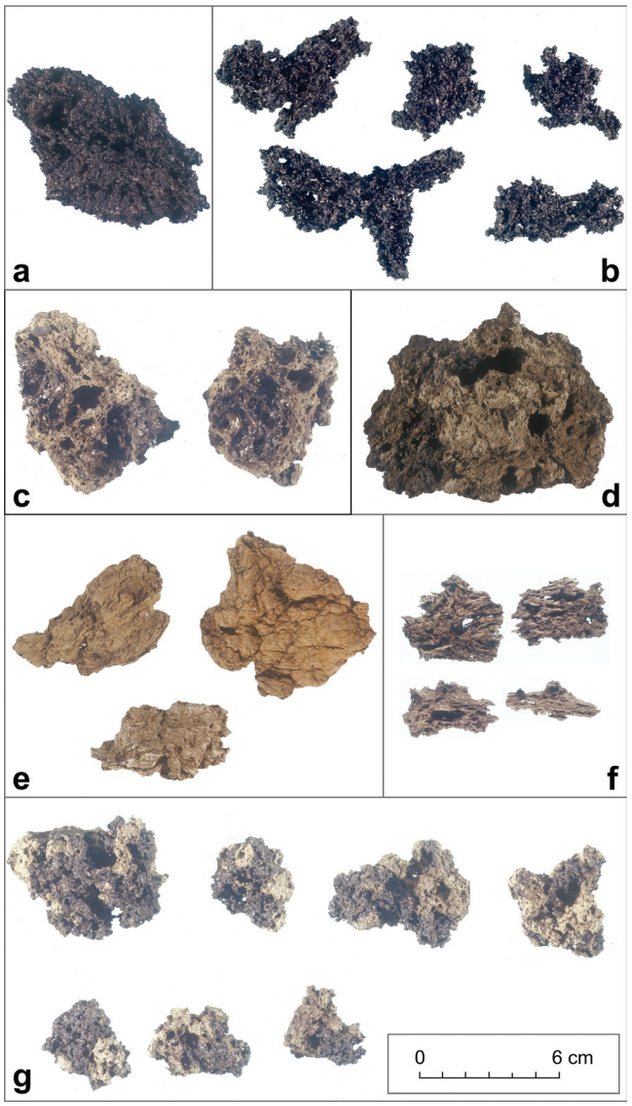

Plate 1. Highly porphyritic (HP) and low porphyritic (LP) juvenile clasts. Black HP scoriae with variable vesicularity (a) and (b); LP pumice showing an external light colored (golden) surface and a black luster interior with large coalescent bubbles (c) or with an only cavity (d); platy LP clasts with smooth microvesicular golden surface (e); highly vesicular fibrous LP clasts (f); mingled HP (dark colored)/LP (light colored part) clasts (g).

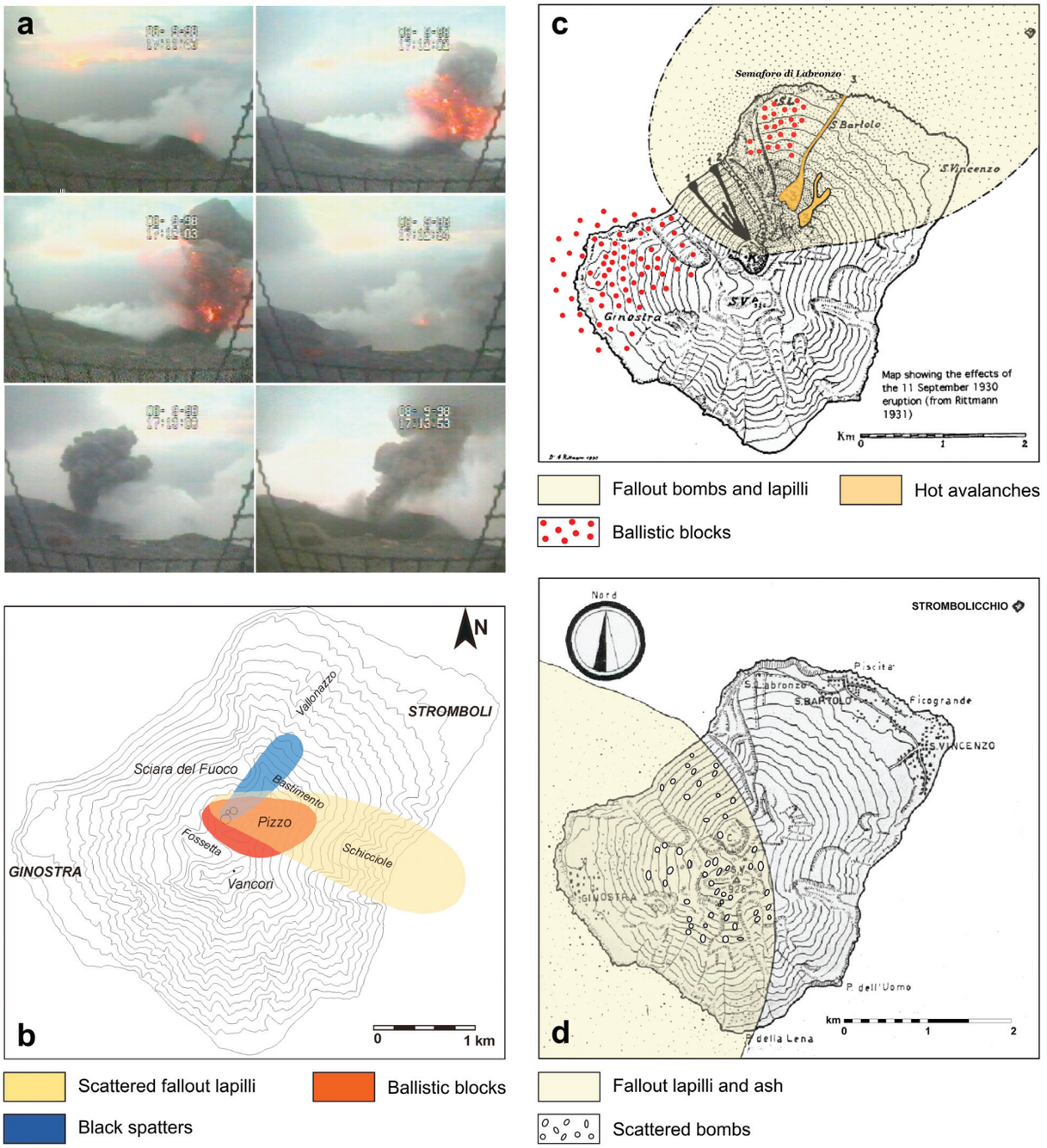

Plate 2. (a) Explosive sequence of a small-scale paroxysm (8 September 1998) as recorded by the surveillance camera at Pizzo, located about 250 m from the Crater Terrace [from *Bertagnini et al.*, 1999]. Product dispersal during: (b) small-scale paroxysm (23 August 1998, modified from *Bertagnini et al.* [1999]), (c) large-scale paroxysm (11 September 1930, modified from *Rittmann* [1931]), (d) intermediate-scale paroxysm (9 July 1959, modified from *Cavallaro* [1962]).

The presence of golden pumices characterizes all the large-scale paroxysms and most of the smaller ones [*Barberi et al.*, 1993; *Bonaccorso et al.*, 1996; *Bertagnini et al.*, 1999, 2003; *Coltelli et al.*, 1999; *Francalanci et al.*, 1999, 2004; *Rosi et al.*, 2000, *Métrich et al.*, 2001, *Bertagnini et al.*, 2003]. In some small-scale events (e.g., 8 September 1998; 20 October 2001; 23 January 2002 [*Bertagnini et al.*, 1999; *Calvari et al.*, 2002], only black crystal-rich scoria and/or lithic clasts were emitted without any evidence of pumices. Lithic clasts are represented both by scoria and lava with hydrothermal and fumarolic alteration and fresh lava fragments [*Ponte*, 1921; *Rittmann*, 1931].

3. MINERALOGICAL, CHEMICAL, AND ISOTOPIC CHARACTERISTICS OF PRODUCTS FROM THE PRESENT-DAY ACTIVITY

Over a period of about 1500 years, the eruptive products of Stromboli show a net bimodality in the characteristics of the erupted magmas as testified by the emission of crystal-rich/volatile poor [highly porphyritic (HP)] magmas erupted as scoria and lava and crystal-poor/volatile-rich [low porphyritic (LP)] magmas erupted as pumice. The LP pumice/HP scoria pairs have fairly similar bulk major element compositions, but distinctive textures, crystal, and volatile contents, matrix glass, and Sr isotope compositions [*Métrich et al.*, 2001; *Bertagnini et al.*, 2003; *Francalanci et al.*, 1999, 2004; *Landi et al.*, 2004; *Francalanci et al.*, 2005].

3.1. Highly Porphyritic (HP) Magma

The HP magma feeding the normal Strombolian activity and the effusive events is a HK/shoshonitic basalt (in wt %: $48.5 < SiO_2 < 51.5$; $1.9 < K_2O < 2.5$; $CaO/Al_2O_3 = 0.59–0.62$) (Figure 3), containing 45–55 vol % of euhedral crystals including plagioclase (0.1–2.5 mm), clinopyroxene (0.5–5 mm), and olivine (0.1–4 mm).

Plagioclase is the most abundant phase (33 vol % on average) with a compositional mode at An_{68} (Figure 4a). They show concentric zoning with alternating layers of (1) labradoritic plagioclase (An_{60}–An_{70}) and (2) sieved textured, patchy zoned plagioclase (An_{70}–An_{90}) rich in melt inclusions and voids which commonly grow on dissolution surfaces. These characteristics are related to repeated episodes of resorption and growth events under high undercooling, [*Landi et al.*, 2004]. Their outer rims, which are in textural equilibrium with the groundmass have labradoritic composition ($An_{64–70}$). The clinopyroxene represents ~12% volume. Its composition ranges from Fs_5 to Fs_{18} [$Wo_{38–48}$, magnesium number, Mg # = Mg/(Mg + Fe^{2+}) 0.91–0.69], showing two distinct modes at $Fs_{12–15}$ and $Fs_{6–9}$ (Figure 4b). The MgO-rich

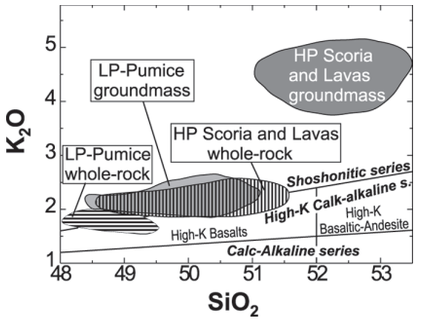

Figure 3. Compositional fields, reported in the K_2O versus silica classification diagram [*Peccerillo and Taylor*, 1976] for the whole rocks and the glassy groundmasses of products erupted in the period 1900–2002. HP, highly porphyritic; LP, low porphyritic. Data are plotted on water-free bases. Data are from *Métrich et al.* [2001], *Francalanci et al.* [2004, 2005] and *Landi et al.* [2004].

component ($Fs_{5–10}$) is subordinate and occurs only as rounded cores and/or intermediate thin layers with rounded surfaces. Fe-rich clinopyroxene (Fs > 15, Wo < 40 mol %) is also present as rare corroded cores. The two clinopyroxene groups (Figure 4b) are also distinguished on the basis of minor element contents. The group at lower Fs contents shows higher Cr content, lower Mn and Ti abundances, and well-defined correlations of Mg # with Al_{tot}, Mn, Ti, and Cr. This characteristic suggests different mineral/liquid equilibrium [*Francalanci et al.*, 2004]. Olivine (~5 vol %) generally shows a restricted compositional range between $Fo_{70–73}$. Resorbed crystals with <10 μm rims of $Fo_{74–75}$ are sporadically found. Finally, glomeroporphyritic aggregates up to 6–7 mm in diameter are common. They are made up of the same mineral phases sometimes associated to small interstitial plagioclase. The compositional ranges of plagioclase, clinopyroxene, and olivine do not show systematic variations with time since the beginning of the 20th century [*Francalanci et al.*, 2004; *Landi et al.*, 2004].

Crystal size distribution (CSD) of scoria and lavas emitted over the last 20 years [*Armienti et al.*, 2007] shows a linear dependence from the crystal size with quite constant slopes and intercepts, revealing a system that is close to the equilibrium from a kinetic point of view. The linear crystal size distribution, particularly for plagioclase, is reached through recurrent episodes of growth and resorption.

In summary, the systematic mineralogical study of scoriae and lavas, produced since the beginning of the present-day activity, testifies to the systematic prevalent crystallization of plagioclase An_{68}, in equilibrium with olivine $Fo_{71–73}$, clinopyroxene $Fs_{12–15}$, and the shoshonitic residual melt. Compositions of glassy to hypocrystalline groundmasses

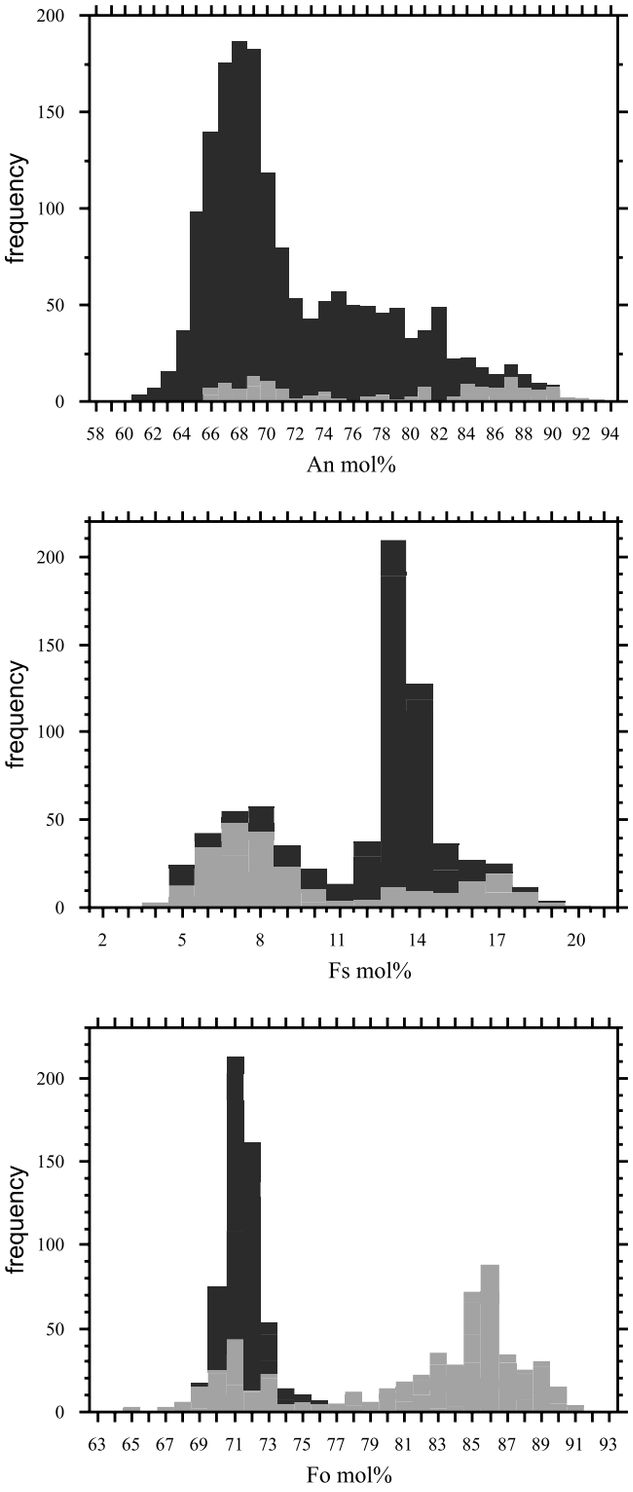

are shoshonitic basalts and shoshonites (Figure 3). Extensive analyses of the glassy matrices erupted over the last 100 years prove their chemical homogeneity [*Landi et al.*, 2004; *Lautze and Houghton* 2005].

Detailed geochemical analyses on products emitted during the 19th century suggest a slight increase of the mafic character of the HP magma between 1906 and 1930 (e.g., MgO: 5 to 6.5 wt %, Ni: 28 to 58 ppm; Table 1; Figure 5a), and then a decrease after 1965 [*Francalanci et al.*, 2004]. A different behavior is observed for the incompatible trace element contents (especially for Ba, Sr, Rb, Nb, and light REE), which are more enriched after 1930 (e.g., Ba > 900 ppm, Sr > 650 ppm, Nb > 18 ppm; Table 1; Figure 5b). This increase of incompatible trace element contents was attributed to a compositional variation in the replenishing LP magma [*Francalanci et al.*, 2004].

Sr isotope ratios in scoria and lavas from the beginning of the 20th century to around 1980–1985 are constant with an average of 0.70626 (±2, 2σ), then start to smoothly decrease down to a value of 0.70616 in June 2002 scoria. This time variation was used to calculate a short residence time (≈19 ±12 years) of the HP magma feeding the present-day activity (Figure 5c). Nd isotope ratios since 1996 are more homogeneous (0.51255–0.51256) than $^{87}Sr/^{86}Sr$ variation [*Francalanci et al.*, 1999, 2004].

3.2. Low Porphyritic (LP) Magma

The LP magma is erupted as pumice during paroxysms. The bulk pumices are HK-basalts (in wt%: $48 < SiO_2 < 0$; $1.6 < K_2O < 2.2$; Table 1, Figure 3), carrying about 10 to 30 vol % crystals composed of plagioclase $An_{64–90}$, clinopyroxene $Fs_{5–17}$, $Wo_{48–38}$, and olivine $Fo_{65–91}$. These crystals are in large proportion xenocrysts whose textures indicate negligible to extensive and repeated interactions with volatile-rich melts.

Most of the xenocrysts (plagioclase, clinopyroxene, and olivine) are entrained from HP magma body during its syn-eruptive mingling with the ascending LP magma. They represent the majority of the crystals in grain-sizes > 1 mm and also occur in smaller grain-sizes [*Bertagnini et al.*, 1999; *Métrich et al.*, 2001]. Crystals ultimately entrained at time of eruption are rimmed by the typical shoshonitic residual glass or by thin reaction and growth rims. In contrast, other crystals show extensive reverse and/or oscillatory zon-

Figure 4. (Opposite) Cumulative compositional distribution of (a) plagioclase (in An mol %), (b) clinopyroxene (in Fs mol %), and (c) olivine (in Fo mol %). Black bars: crystal-rich scoria and lavas (HP); gray bars: crystal-poor pumice (LP) [data from *Métrich et al.*, 2001; *Francalanci et al.*, 2004; *Landi et al.*, 2004; *Bertagnini et al.*, 2003; *Métrich et al.*, 2005; *Landi et al.*, 2006].

Table 1. Whole Rock Compositions of Selected Scoria, Lava and Pumice Representative of the Magma Feeding the Present Activity of Stromboli

	HP												
Sample	St82s[a] Hist.	St79s[a] Hist.	ST06[b] 1906	ES21[b] 15/3/14	ES281[b] 1929	ES204[b] 11/9/30	ES203[b] 11/9/30	ST65.2[b] 1965	Sr1[c] 12/11/75	ST346[b] 1983	STR45[d] 28/4/84	STR202[d] 12/12/85	Sr7[b] 17/4/86
Date	Scoria	Scoria	Scoria	Lava	Lava	Scoria	Scoria	Scoria	Lava	Scoria	Scoria	Lava	Lava
SiO_2	51.07	52.50	51.31	51.44	50.77	50.87	50.71	50.23	49.47	50.03	51.03	49.62	49.25
TiO_2	0.9	0.84	0.91	0.92	0.82	0.84	0.84	0.89	0.96	0.89	0.94	1.00	1.01
Al_2O_3	17.13	16.81	17.72	18.01	16.68	17.04	17.23	16.55	18.47	17.28	17.66	18.07	17.76
Fe_2O_3	3.1	3.13	2.64	2.86	3.61	2.34	3.93	2.59	3.13	2.64	2.65	3.52	2.57
FeO	5.18	4.76	5.45	5.32	4.39	5.69	4.31	5.43	5.22	5.55	5.39	5.31	6.24
MnO	0.16	0.15	0.16	0.15	0.15	0.15	0.15	0.16	0.17	0.15	0.15	0.16	0.18
MgO	6.58	6.07	5.16	5.04	6.49	6.44	6.35	6.65	5.50	6.30	5.80	6.01	6.08
CaO	10.59	9.91	10.31	10.11	11.33	11.33	11.05	11.68	11.17	11.20	10.62	11.00	11.16
Na_2O	2.42	2.42	2.74	2.93	2.57	2.52	2.61	2.52	2.68	2.66	2.50	2.42	2.51
K_2O	1.92	1.93	2.28	2.32	2.05	2.09	2.03	2.21	2.14	2.25	2.22	1.98	2.13
P_2O_5	0.39	0.37	0.53	0.52	0.47	0.48	0.50	0.58	0.41	0.56	0.48	0.57	0.41
H_2O	0.56	1.11	0.40	0.35	0.62	0.25	0.30	0.54	0.68	0.48	0.50	0.27	0.70
Sc			21.0	19.0	22.0	26.0	24.0	25.0	32.2	26.0			30.0
V	256	246	281	296	295	303	299	283	274	281	270		274
Cr	107	84	17	29	23	104	81	110	85	74	78	86	67
Co	31	30	36	33	40	33	37	42	34.1	35	33	34	34.6
Ni	44	46	30	27	52	47	48	53	39	41	42	38	42
Rb	65	66	69	71	61	61	59	63	81	62	74	80	82
Sr	716	687	662	633	632	628	637	717	789	660	736	762	740
Y	25	25	27	25	24	27	26	27	27	26	28	28	28
Zr	151	143	190	167	150	153	157	194	163	165	162	166	161
Nb	18	18	19	17	17	17	18	19	23	18	22	23	22
Cs	5.2	5.1											
Ba	915	910	880	896	818	861	867	1003	1088	911	1023	1004	988
La	46	44	46	48	49	60	39	59	49.4	63	50	52	47
Ce	89	87	94	134	101	95	113	109	100	113	97	99	98
Pr	10.4	10.3											
Nd	41	39	39	44	42	35	47	44	49	42	45	40	42
Sm	7.8	7.6							8.5			9.4	8.8
Eu	2.0	2.0							2.30			2.10	2.10
Gd	5.9	6.3											
Tb	0.86	0.90							0.83			1.00	1.10
Dy	4.98	4.80											
Ho	0.90	0.89											
Er	2.18	2.27											
Tm	0.31	0.36											
Yb	2.18	2.04							2.9			2.6	2.7
Lu	0.33	0.30							0.36			0.45	0.36
Hf	3.5	3.4							3.5			3.9	3.7
Ta	1.14	1.05							1.4			1.3	1.5
Pb	17	16							47		16	21	20
Th	17.2	14.3							16.2		16	15.9	16.6
U	3.82	3.90											
$^{87}Sr/^{86}Sr$			0.706271	0.706256	0.706271	0.706264		0.706260	0.706212	0.706208	0.706191	0.706228	0.706199
$^{143}Nd/^{144}Nd$													

Table 1. (continued)

	HP						LP						
Sample	ST89.0[b]	Str93-1[e]	STR9/95c[f]	STR9/96e[f]	ST133s[a,*]	ST182[g]	ST82p[h]	ST79p[h]	ST81p[h]	Str93-2[e]	STR9/96d[f]	ST140p[a,*]	ST178[h]
Date	1989	10/2/93	27/9/95	4/9/96	23/8/98	26/8/99	Hist.	Hist.	Hist.	10/2/93	4/9/96	23/8/98	26/8/99
	Scoria	Scoria	Scoria	Scoria	Scoria	Scoria	Pumice	Pumice	Pumice	Pumice	Pumice	Pumice	Pumice
SiO_2	50.63	49.91	49.30	49.52	49.89	50.40	50.87	51.51	51.61	49.13	48.59	49.05	50.01
TiO_2	0.87	0.99	0.97	0.96	0.98	0.95	0.9	0.87	0.87	1.02	0.99	0.97	0.97
Al_2O_3	17.29	17.77	17.93	18.07	18.05	17.83	16.56	16.67	16.22	17.08	16.31	17.14	17.14
Fe_2O_3	2.89	1.82	2.58	2.87	3.86	2.48	3.46	3.01	3.01	4.18	3.60	4.6	2.56
FeO	5.17	6.63	6.08	6.00	4.9	5.88	5.11	5.10	5.4	5.09	5.75	4.4	6.16
MnO	0.16	0.16	0.16	0.17	0.16	0.16	0.16	0.15	0.16	0.17	0.18	0.16	0.16
MgO	6.22	6.30	6.57	6.08	5.97	6.27	6.66	6.34	6.64	6.25	7.84	6.93	6.37
CaO	11.05	10.87	11.17	11.21	10.78	10.73	10.91	10.34	10.61	12.21	12.21	11.59	11.24
Na_2O	2.54	2.51	2.47	2.49	2.6	2.52	2.39	2.75	2.45	2.30	2.05	2.38	2.51
K_2O	2.16	2.07	2.04	2.08	2.07	1.97	1.82	2.21	1.87	1.65	1.68	1.62	1.75
P_2O_5	0.47	0.45	0.38	0.38	0.45	0.44	0.4	0.39	0.38	0.45	0.37	0.42	0.46
H_2O	0.31	0.52	0.34	0.17	0.28	0.33	0.77	0.66	0.79	0.48	0.43	0.73	0.60
Sc			33.2	32.2	30						35.9		
V	258		269	280	264	264	270	249	247		287	278	259
Cr	90	49	76	62	49	55	116	132	98	38	54	51	36
Co			35	32	33	31	34	31	32		36.6	34	33
Ni	44	35	35	36	41	34	51	49	44	37	46	46	37
Rb	63	67	78	82	66	65	62	73	63		66	52	55
Sr	682	707	753	757	734	708	742	756	728	720	748	701	721
Y			24	28	27	25	24	25	24		27	26	25
Zr	175		174	161	152	153	148	164	146		142	132	141
Nb		25	20	21	19	18	18	20	18	18	19	16	15
Cs					4.9	4.2	4.6	5.5	4.4			3.7	3.5
Ba	938		971	998	956	912	901	982	954		818	816	848
La			50	50	45	44	45	47	49		42	39	42
Ce			98	97	91	89	88	92	96		87	81	84
Pr					10.8	10.8	10.5	10.6	11.3			9.8	9.9
Nd			38	39	42	43	40	42	42		34	39	39
Sm			9.4	9.0	8.1	8.5	7.5	8.2	8.5		8.2	7.8	7.9
Eu			2.26	2.22	2.0	2.2	2.0	2.1	2.2		2.10	2.0	2.2
Gd					7.0	6.7	6.3	6.3	6.2			6.7	6.4
Tb			1.10	0.95	0.98	0.93	0.84	0.84	0.90		0.93	0.95	0.92
Dy					5.30	4.94	4.56	4.63	4.72			4.90	4.88
Ho					0.98	0.97	0.87	0.83	0.88			0.92	0.88
Er					2.65	2.25	2.19	2.24	2.45			2.44	2.21
Tm					0.38	0.35	0.32	0.34	0.31			0.36	0.3
Yb			2.8	2.4	2.26	2.28	2.11	2.07	2.36		2.4	2.10	2.19
Lu			0.46	0.5	0.33	0.34	0.29	0.31	0.35		0.48	0.31	0.31
Hf			3.7	3.7	3.6	3.7	3.1	3.4	3.5		3.2	3.2	3.2
Ta			1.7	1.5	1.09	1.20	1.07	1.22	1.22		1.14	0.90	1.03
Pb			27	23	17	17	16	18	18		20	14	14
Th		9	17	17	14.4	14.3	15.6	18.2	15.0	7	13	11.4	11.9
U					3.70	3.78	3.45	4.13	3.91			2.88	2.96
$^{87}Sr/^{86}Sr$	0.706248		0.706162	0.706165	0.706160						0.706105	0.706107	
$^{143}Nd/^{144}Nd$				0.512556	0.512551						0.512570	0.512564	

(Hist) historical activity from (a) *Métrich et al*. [2001]; (b) *Hornig-Kjarsgaard et al*. [1993]; (e) *Bonaccorso et al*. [1996]; (f) *Francalanci et al*. [2004]; (g) *Landi et al*. [2004]; (h) *Bertagnini et al*. [2003]. (*) isotopic compositions from *Francalanci et al*. [2004].

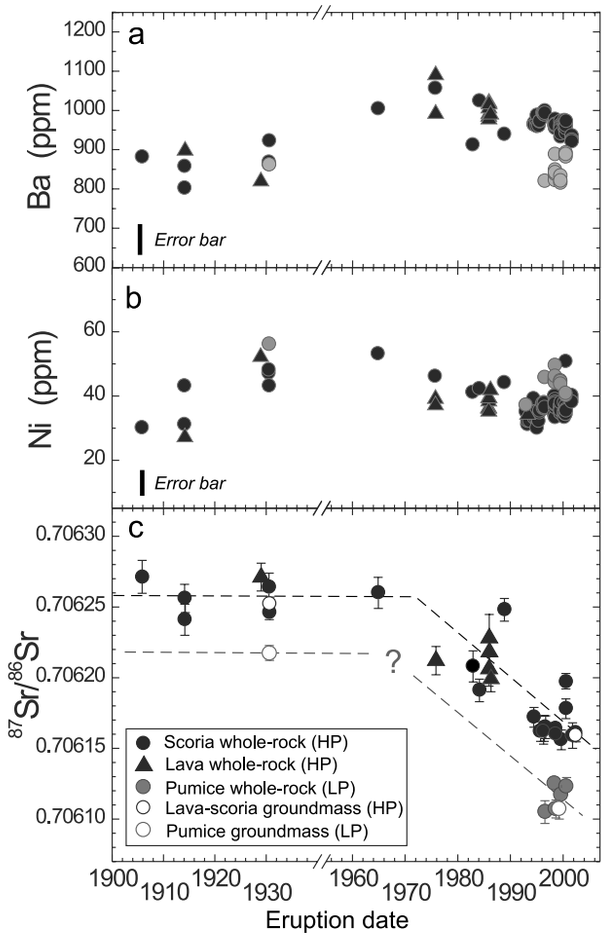

Figure 5. Compositional variations with time for the products erupted in the period 1906–2002. (a) and (b) Ni and Ba variations reported as representative of compatible and incompatible trace elements, respectively. Error bars are generally referred to errors of ~5% for Ba and ~10% for Ni calculated at the average composition of the studied rocks [data from *Francalanci et al.*, 2004 with reference therein and unpublished]; (c) Sr isotope ratio variations with reported 2σ errors [data from *Francalanci et al.*, 1999, 2004, 2005] HP and LP indicate highly porphyritic and low porphyritic products, respectively.

ing, dissolution surfaces, successive reequilibration events and growth rims of variable thickness (Figures 6a and 6b). Similar features are also observed in clinopyroxene. Crystals that record extensive disequilibria dominate in pumice erupted during small-scale paroxysms as what occurred in August 1998 and 1999 [*Métrich et al.*, 2001; *Bertagnini et al.*, 2003].

Actually, the mineral paragenesis of pumice consists in small (<1 mm) and scarce (<5 vol %) diopside (Fs_{8-5}, Wo_{48-45}) and skeletal or euhedral homogeneous olivine (Fo_{82} to Fo_{87}), with numerous irregular melt inclusions (Figure 6c). Skeletal Ca-rich plagioclase (An_{80-92}) is frequently found as reaction and growth rims surrounding xenocrystic relicts and results from the final stages of crystallization. In addition, pumices of the large-scale paroxysms systematically contain MgO-rich olivine (Fo_{88-91}) as homogeneous, normally or reversely zoned, skeletal or composite crystals (Figure 6d). Their composition and association with Cr-spinel (Cr # 64–67, Mg # 59–67) testify to their derivation from more primitive melts. Systematic chemical profiles in reversely zoned olivine crystals indicate variable times of crystal–magma interaction that is of the order of a few hours to weeks before the eruption [*Bertagnini et al.*, 2003].

The pumice samples display bulk rock compositions quite similar to those of scoriae and lavas erupted in the same period, with only slightly lower incompatible and higher compatible element contents (Table 1, Figures 5a and 5b). In contrast, the pumice matrix glasses are HK/SHO-basalts with distinctive less evolved compositions than those of the HP scoria and lavas [*Métrich et al.*, 2001; *Francalanci et al.*, 2004].

Although the LP pumices emitted in the 20th century have major and trace element contents similar to those of the coeval HP scoria, they show significantly lower Sr isotope ratios than scoriae. In addition, a significant variation of Sr isotope ratios has been also found in LP pumices. More, specifically, the LP pumices emitted in 1930 have $^{87}Sr/^{86}Sr$ values higher than the younger pumices (since 1984 onward). These data suggest a variation with time similar to that of HP magmas (Figure 5c). The $^{143}Nd/^{144}Nd$ values of LP pumices erupted since 1996 do not significantly differ from those of coeval HP magmas, showing only slightly higher values (0.51256–0.51257) [*Francalanci et al.*, 1999, 2004, 2005].

4. CONTRIBUTIONS FROM MICROANALYTICAL Sr ISOTOPE DATA

Detailed microanalytical Sr isotope analyses were performed by microdrilling techniques on largely zoned plagioclase and clinopyroxene and groundmasses on four samples (an HP scoria erupted in 1984, a lava sample of the 1985–1986 event, HP scoria and LP pumice of the 1996 small-scale paroxysm) [*Francalanci et al.*, 2005].

Large and comparable Sr isotope variations have been detected in plagioclase and clinopyroxene. The resorbed cores of crystals from HP magmas show high $^{87}Sr/^{86}Sr$ (0.70635–0.70630) or low $^{87}Sr/^{86}Sr$ (0.70614–0.70608), with the latter values similar to the values of the outer cores. Mineral rims and glassy groundmasses generally have intermediate $^{87}Sr/^{86}Sr$ (0.70628–0.70613; Figure 7). Three groups of $^{87}Sr/^{86}Sr$

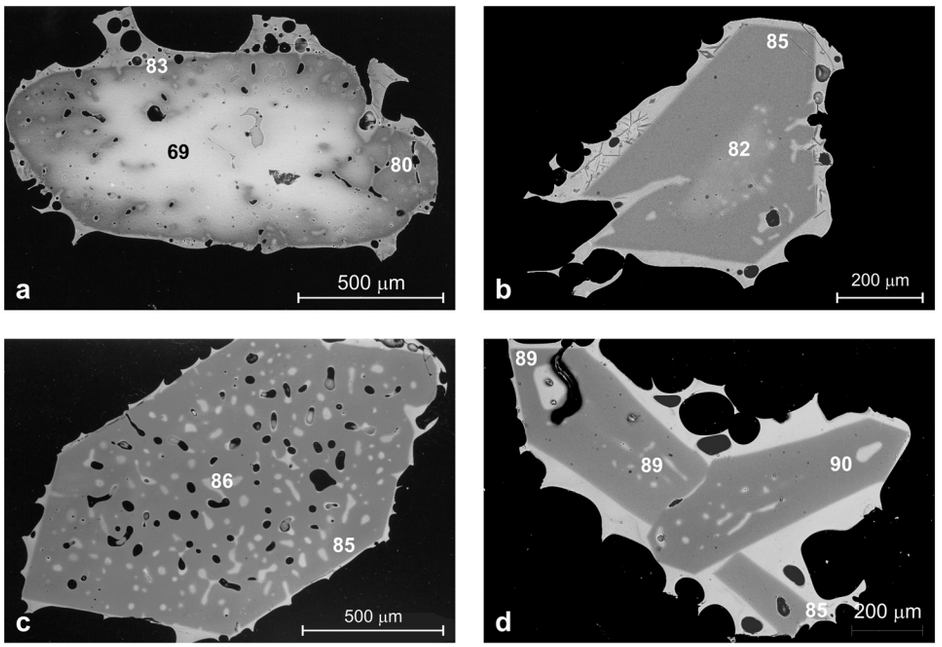

Figure 6. Back-scattered electron micrographs of olivines from LP pumice. (a) Fe-rich resorbed core surrounded by a heterogeneous mottled zone rich in MI (large-scale historical paroxysm, St79 sample); (b) reverse zoned crystal with a large and homogeneous growth rim and skeletal shape (small-scale paroxysm of 23 August 1998, St130 sample); (c) homogeneous euhedral olivine showing high density of irregular elongated melt inclusions (large-scale historical paroxysm, St82 sample); (d) skeletal crystals of Mg-rich olivine (large-scale historical paroxysm, St82 sample).

values also characterize the mineral growth zones from the LP magmas, but the lowest values are present in the mineral rims and groundmass glass. In minerals of scoria/pumice pair from 1996 paroxysm, the low Sr-isotope values are comparable, and in HP magmas, Sr isotope ratios increase toward the external zones of phenocrysts (with the intermediate isotope values) starting from the lowest $^{87}Sr/^{86}Sr$ ratios of cores and/or outer cores. Furthermore, the crystal zones with the lowest and intermediate Sr isotope ratios have the main compositions typical of minerals in equilibrium with LP magmas and HP magmas, respectively (Figure 7). This clearly indicates that the external zones of plagioclase and clinopyroxene from scoria and lavas crystallized concurrently with, or after, mingling/mixing between the LP and HP magmas.

Finally, the usually resorbed, mineral cores with high $^{87}Sr/^{86}Sr$ values have been considered to represent a third component in the plumbing system, such as a cumulus crystal-mush zone, situated just below the shallow magma reservoir and associated with the more Sr-radiogenic feeding system of the preceding volcanic activity. It is proposed that the cumulus phases are incorporated by the LP magma ascending from depth and transported into the shallow reservoir [*Francalanci et al.*, 2005].

The micro-Sr isotope data have also suggested a rapid decrease of $^{87}Sr/^{86}Sr$ in the replenishing LP magma before the eruption of the 1985 lava flow, associated with an increased volume of LP magma into the shallow magma reservoir [*Francalanci et al.*, 2005].

5. CONTRIBUTIONS FROM MELT INCLUSIONS

5.1. Textural Aspects

Specific attention has been paid to olivine-hosted melt inclusions from scoria and pumice that show a large spectrum in morphology and composition. As a result, a large chemical data set on melt inclusions and their host crystals was published in *Métrich et al.* [2001] and *Bertagnini et al.* [2003]. Melt inclusions in clinopyroxene are often crystallized, and only a few major element compositions have been published [*Clocchiatti*, 1981]. Rapid growth of plagioclase and its recurrent dissolution prevent reliable analysis of their entrapped glasses [*Landi et al.*, 2004].

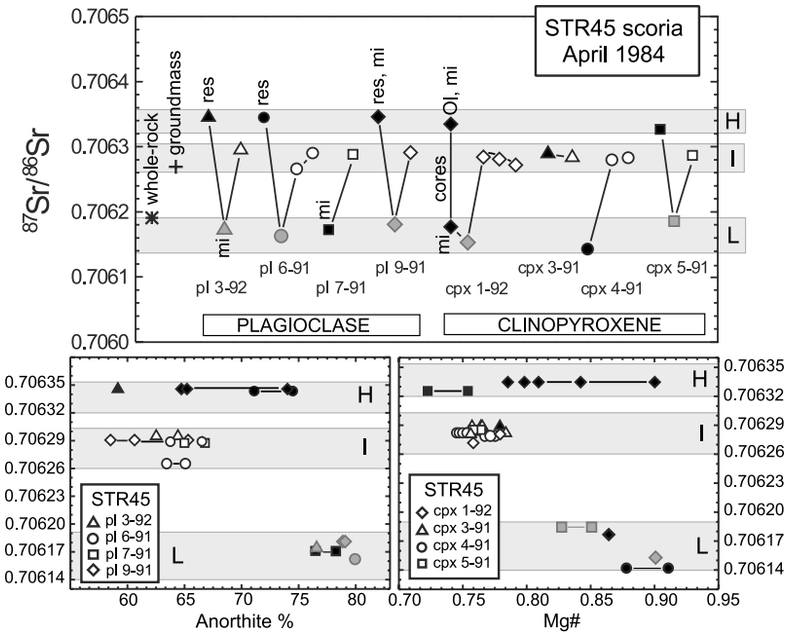

Figure 7. Sr isotope data of HP scoria (erupted by normal Strombolian activity on 28 April 1984) measured in whole-rock, glassy groundmass and core-rim traverses of plagioclase and clinopyroxene. Each mineral is reported with a different symbol. From left to right of each mineral of the above diagram: from core (filled symbol), to outer core (grey symbol), up to outer rim (open symbol). The two diagrams below show that the high Sr-radiogenic crystal zones (H) have variable composition, the low Sr-radiogenic crystal zones (L) always have high anorthite contents or magnesium number [Mg #=Mg/(Mg + Fe^{2+})], whereas the zones with intermediate Sr isotope ratios (I) usually have intermediate anorthite contents or Mg #. Res, resorbed, mi, with melt inclusions. The 2σ error corresponds with the symbol size. Modified after *Francalanci et al*. [2005].

Scoriae of normal Strombolian activity contain euhedral Fe-rich olivine with melt inclusions that are regularly distributed along the crystal growth boundaries. Melt inclusions rarely exceed 25–30 μm in size. They contain at most one shrinkage bubble; few of then contain tiny, Cu–Fe sulfide globules.

The large-scale historical paroxysms bring to surface a range of olivine crystals and melt inclusions whose morphology indicates successive dissolution–crystallization events, multistage crystallization, dynamic mixing upon magma ascent [*Bertagnini et al.*, 2003]. One can observe morphological evolution from typical isolated, two-phase inclusions in the Mg-rich olivines ($Fo_{88–90}$) toward irregular elongated and interconnected melt inclusions in more Fe-rich olivine ($Fo_{82–87}$; Figure 6c). The high density of trapped glass, without any preferential orientation, together with variable proportions between bubble and glass often attest to very rapid growth rates of the host from a heterogeneous gas–melt mixture.

5.2. Major Element and Volatile Compositions and Optical Thermometry

Melt inclusions and matrix glasses define a compositional trend that is far wider than that of the whole rocks (Figures 8a and 8b). More specifically, in scoriae, olivine-hosted melt inclusions are evolved (CaO/Al_2O_3 = 0.6–0.4) and are closely comparable in composition to the shoshonitic matrix glass. Their decreasing K_2O/Na_2O ratio and Al_2O_3 content testify to plagioclase crystallization in accordance with their low water content. Melt inclusions in olivine ($Fo_{71–73}$) contain 0.05–0.6 wt % H_2O [*Métrich et al.*, 2001] although water loss through olivine network cannot be totally excluded. As a whole, the volatile content in melt inclusions from scoriae is low (CO_2 < 100 ppm; dl > S < 1300 ppm; Cl = 1000–2600 ppm), except fluorine (1000–1300 ppm; *Métrich et al.* [2001]). Finally, the temperature of crystallization of the HP magma was determined at 1115 ± 10ºC from optical thermometry measurements in melt inclusions

in clinopyroxene and olivine [*Clocchiatti*, 1981; *Métrich et al.*, 2001].

In pumice, olivine-hosted melt inclusions recorded a compositional range extending from HK-basalt akin to those of pumice bulk rocks and glassy matrices to Ca-rich compositions (Figure 8a; Table 2). The latter, recorded as melt inclusions in $Fo_{88–90}$ that are entrained during the large-scale paroxysms, are regarded as representative of the possible parental melts (CaO/Al_2O_3 ~1) of the magma batches (CaO/Al_2O_3 ~0.65) feeding the present activity. They have slightly variable K_2O content. Accordingly, the bulk pumice compositions were explained by the removal of nearly 24% solid, made up of clinopyroxene and minor olivine, from the parental Ca-rich melt(s) [*Bertagnini et al.*, 2003]. The temperature of crystallization of the Stromboli LP magma ranges from 1200º to 1135 ± 10ºC as estimated using MELTS code [*Bertagnini et al*., 2003] and microthermometry measurements on melt inclusions [*Métrich et al.*, 2001], respectively.

Melts trapped in heterogeneous olivine that recorded dissolution–crystallization events were systematically identified, but never considered as representative of the magma system and never reported in diagrams showing the typical trend of magma evolution at Stromboli. This type of melt inclusion and olivine dominates (>95% of crystals from the 0.5- to 1-mm grain-size fractions; regardless of crystals entrained from the HP magma) in pumice produced by small-scale paroxysms (e.g., eruptions of August 1998 and August 1999).

Melt inclusions in olivine $Fo_{82–90}$ yield high volatile content (in wt %: H_2O = 1.8–3.4, CO_2 = 890–1890 ppm, S = 1660–2250 ppm, Cl = 1660–2030 ppm; F = 640–680 ppm; *Métrich et al.* [2001] and *Bertagnini et al.* [2003]) (Table 3). Prior to significant degassing, basaltic magma(s) at Stromboli are characterized by a S/Cl ratio of 1.1 ± 0.1 (Figure 8c) and a F/Cl ratio of between 2.5 ± 0.2 on average. The high water content in pumice-forming melts inhibits plagioclase crystallization in agreement with experimental phase equilibria [*Di Carlo et al.*, 2006]. Plagioclases often observed in pumice are inherited from the HP magma and/or have

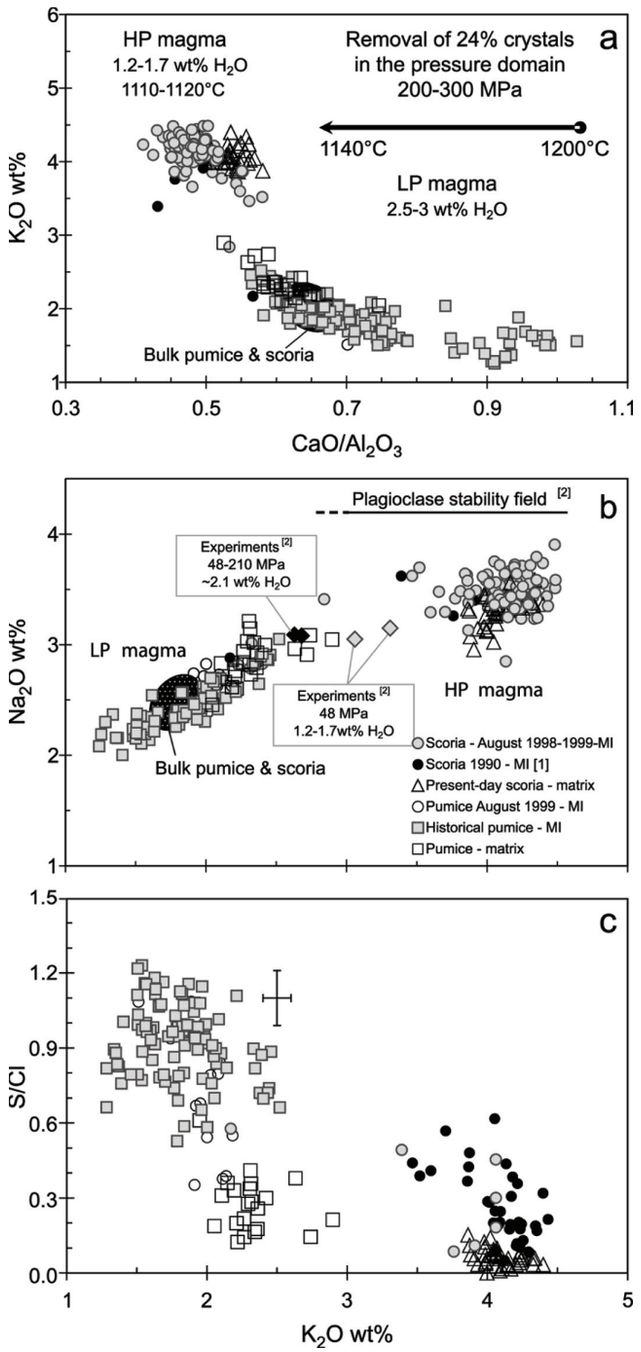

Figure 8. (Opposite) (a) Synthetic diagram [modified from *Bertagnini et al.*, 2003] showing the evolution of CaO/Al_2O_3 versus K_2O, with pressure and temperature of olivine-hosted melt inclusions and of matrix glasses in pumices (samples ST81, 82, 79, 207) emitted during large-scale historical paroxysms and of pumices and scoriae produced during the 1998–1999 small-scale paroxysms. The compositions of the whole rocks (scoria and pumice) and of experimental melts are reported for comparison (see text for details). The temperatures of crystallization are either determined by microthermometry on melt inclusions [*Métrich et al.*, 2001] or calculated using MELTS code [*Ghiorso and Sack*, 1995]. The pressures are derived from the H_2O and CO_2 dissolved content of melt inclusions using Volatilecalc (see text); (b) variation of K_2O versus Na_2O and (c) evolution of the S/Cl ratio versus K_2O in olivine-hosted melt inclusions and matrix glasses of Stromboli pumice and scoria. [1] and [2] are from *Allard et al.* [1994] and *Di Carlo et al.* [2006], respectively.

Table 2. Selected Analyses of Melt Inclusions in Olivine of Pumice and Scoria

Sample	St81[a]	St207[a]	St82p[b]	St79p[b]	St81[a]	St81[a]	St82p[b]	St79s[b]	St82s[b]	St133s[b]
Inclusion	Ol 11	Ol a5	Ol 11	Ol n30	Oln10	Ol 8	Ol n50	Ol n14	Ol n2	Ol 10
No. of analysis	Mean (20)	MI 1 (3)	Mean (14)	Mean (12)	Mean (12)	MI 1 (3)	MI a (3)	MI a,b,c (4)	MI 2 (2)	MI 2 (2)
SiO2 (wt%)	47.66	47.74	47.73	47.31	48.47	48.33	49.29	49.36	52.85	51.47
TiO_2	0.89	0.91	0.83	0.86	0.82	0.83	0.87	0.83	1.45	1.48
$A1_2O_3$	14.23	14.92	15.64	14.84	15.88	16.60	15.54	16.92	15.16	15.17
FeO_{tot}	7.28	6.19	7.71	6.73	7.22	7.63	8.53	7.42	9.60	11.25
MnO	0.12	0.11	0.14	0.12	0.08	0.23	0.18	0.12	0.18	0.28
MgO	7.64	6.51	7.30	6.89	6.60	6.67	6.03	4.79	3.43	3.92
CaO	14.05	13.84	12.18	14.36	11.48	11.25	10.02	10.01	6.91	6.82
Na_2O	2.27	2.16	2.24	2.28	2.35	2.57	2.44	2.86	3.53	3.40
K_2O	1.58	1.36	1.58	1.61	1.88	1.82	1.97	2.44	3.84	4.10
P_2O_5	0.54	0.54	0.54	0.54	0.50	0.52	0.59	0.59	0.76	1.06
S	0.235	0.150	0.162	0.225	0.175	0.168	0.121	0.129	0.074	0.069
Cl	0.198	0.180	0.169	0.203	0.173	0.174	0.155	0.175	0.226	0.180
Total	96.43	94.34	96.10	95.72	95.63	96.79	95.74	95.64	98.00	98.52
Olivine Fo mol%	88.4	88.7	87.5	88.0	87.0	86.5	83.7	82.3	72.7	72.0
% PEC	0.08	0.05	0.03	0.06	0.07	0.05	0.04	0.07	0.01	0.02
CaO/Al_2O_3	0.98	0.93	0.78	0.97	0.72	0.68	0.64	0.59	0.46	0.52
K_2O/Na_2O	0.70	0.63	0.70	0.71	0.80	0.71	0.81	0.85	1.09	1.18
S/Cl	1.18	0.83	0.96	1.11	1.02	0.96	0.77	0.74	0.33	0.35

Major and volatile elements are corrected for olivine postentrapment crystallization (% PEC). Fo mol% = [100 × Mg/(Fe + Mg)]. [a] From *Bertagnini et al*. [2003]. Analytical techniques in *Métrich et al*. [2001]. [b] From *Métrich et al*. [2001].

crystallized in response to late water degassing at time of eruption.

The dissolved H_2O and CO_2 contents of melt inclusions were used to assess the total fluid ($P_{CO2} + P_{H2O}$) pressures using the model of *Papale* [1999] and Volatilecalc code [*Newman and Lowenstern* 2002]. The models resulted in different pressure estimates because of the paucity of experimental data of CO_2 solubility in water-rich basalts, as discussed

Table 3. Water and Carbon Concentrations in Selected Melt Inclusions in Olivine of Pumice

Sample	Fo,[a] mol%	K_2O,[b] wt%	S,[b] wt%	Cl,[b] wt%	CaO/Al_2O_3	H_2O,[b] wt%	CO_2,[b] ppm
St81[c]							
Oln12-MI1	84.4	1.79	0.169	0.171	0.71	2.0	799
Oln8-MI1	86.1	1.83	0.165	0.167	0.64	2.7	1098
Oln8-MI2	86.3	1.92	0.166	0.170	0.69	2.1	1887
Oln10-MI2	86.7	1.78	0.180	0.175	0.75	2.3	792
Oln10-MI3	86.6	1.82	0.197	0.176	0.76	2.7	1204
Oln10-MI1	86.9	1.84	0.183	0.171	0.73	2.6	1003
Oln10-MI7	87.1	1.94	0.174	0.176	0.73	2.6	762
Oln10-MI6	85.9	1.86	0.170	0.172	0.70	2.5	1008
Oln14-MI1	83.5	2.05	0.148	0.168	0.61	3.2	1117
Oln14-MI2	83.2	2.10	0.152	0.173	0.60	2.8	867
Oln14-MI3	83.7	2.07	0.142	0.170	0.60	2.4	716
St79p[d]							
Oln30	88.0	1.61	0.225	0.203	0.97	2.3	1107
St82p[d]							
Oln52a	84.6	1.73	0.170	0.179	0.73	2.7	1087
Oln50	83.7	1.97	0.121	0.155	0.64	2.7	894

[a] Fo is the host olivine composition as [100 × Mg/(Mg + Fe)]. [b] Concentrations corrected for the post-entrapment crystallisation of olivine. [c] From *Bertagnini et al*. [2003]. [d] From *Métrich et al*. [2001].

in *Bertagnini et al.* [2003]. In order to take into account the influence of magma composition and dissolved water amount on the CO_2 solubility [*Botcharnikov et al.*, 2005], the best pressure estimates were calculated by Volatilecalc program whose SiO_2 contents are derived from the Π coefficient defined by *Dixon* [1997] to be 48 wt %. Hence, the olivine-hosted melt inclusions from large-scale paroxysms were trapped at a total fluid pressure of between 200 and 300 MPa [*Métrich et al.*, 2005]. A similar conclusion was reached more recently by *Di Carlo et al.* [2006]. This lithostatic pressure would correspond to a depth of 7.5–11 km assuming an average rock density of Stromboli basement of 2700 kg m^{-3}.

6. CONSTRAINTS ON THE FEEDING SYSTEM AND DYNAMICS OF THE PRESENT-DAY ACTIVITY

Since its beginning, about 1500 years ago, the persistent activity at Stromboli has been dominated by the interplay between magmas having contrasting density and viscosity: the shallow, crystal-rich, partially degassed magma (HP magma) and the nearly aphyric, volatile-rich, ascending, magma batches of deeper derivation (LP magma). Textural, mineralogical, geochemical, and isotopic data of the emitted products were combined with detailed microanalyses of melt inclusions and minerals to provide a reference data set on the magma-dissolved volatile contents, the path and pressure (depth) of magma crystallization, and its dynamics of ascent.

One of the most outstanding characteristics of the Stromboli magmas is the closely comparable basaltic composition of the scoria/pumice pairs, in spite of a marked difference in their crystal and volatile contents that makes Stromboli a classic example of crystallization driven by water loss [*Métrich et al.*, 2001]. However, slightly chemical differences between scoria and pumice were attributed to crystal fractionation [*Landi et al.*, 2004]. The magma batches (occasionally erupted as pumice) have a high initial water content (2.5–3.0 wt %), regardless of the paroxysm scale or its age [*Métrich et al.*, 2001; *Bertagnini et al.*, 2003]. Actually, their dissolved water content remains high enough to prevent plagioclase crystallization, except at the ultimate stage(s) of their transfer to the surface when the water loss associated with the lower pressure, drives the melt composition toward the stability field of plagioclase. In contrast, plagioclase is the dominant mineral phase of the shallow degassed magma where it crystallizes in equilibrium with clinopyroxene and olivine, in melts having water content ≤1.2–1.7 wt % [*Landi et al.*, 2004; *Di Carlo et al.*, 2006].

Minerals in scoria record strong chemical, isotopic, and textural heterogeneity at the micrometer scale. These recurrent disequilibria provide evidence of repeated and discrete arrivals of water-rich, less radiogenic $^{87}Sr/^{86}Sr$ melts in the shallow system promoting efficient and dynamic water degassing, magma crystallization, and magma mixing [*Francalanci et al.*, 1999, 2004, 2005; *Métrich et al.*, 2001; *Landi et al.*, 2004]. In contrast, their chemistry and crystal size distribution suggest that the shallow crystal-rich body operates as a steady-state system close to the kinetic equilibrium [*Armienti et al.*, 2007]. All these features are reconciled when considering convective motions at different scales in space and time promoting interactions and mixing between magmas initially containing variable volatile contents and isotopic ratios [*Francalanci et al.*, 1999; *Landi et al.*, 2004]. Such ideas are fully consistent with previous findings of convection associated with intrusive degassing, degassed magma sinking [*Allard et al.*, 1994, *Harris and Stevenson*, 1997; *Allard et al.*, this volume], and differential transfer of gas bubble and slug rise through the crystal-rich shallow body [*Burton et al.*, 2007a, 2007b].

The refilling magma batches ultimately derive from their volatile-rich parental melt(s), via crystal fractionation, at a lithostatic pressure of 200–300 MPa as what were derived from the H_2O and CO_2 dissolved content of melt inclusions [*Métrich et al.*, 2001; *Bertagnini et al.*, 2003]. The volume of the crystal-mush associated with deep fractional crystallization processes over the last 1500 years was assessed on the order of 3.5–7 km^3 [*Bertagnini et al.*, 2003]. According to these authors, the magma ponding zone is located at ~7.5–11 km depth. In this model, the chemical evolution of magma is driven by crystal fractionation in this range of lithostatic depths, whereas crystallization driven by water loss prevails in the shallow reservoir that sustains normal Strombolian activity. Such processes clearly involve mixing between magmas having similar major and trace element bulk composition but different temperature, volatile content, and Sr-isotopic ratios. Actually, the dynamics of water loss and crystallization accounts for the absence of a transition between the crystal-poor and the crystal-rich magma. The evidence of their interaction only survives in mineral zoning and their Sr isotopic ratios.

A model of a polybaric multireservoir plumbing system at Stromboli has been proposed by *Francalanci et al.* [1999, 2004, 2005] and *Vaggelli et al.* [2003] on the basis of extensive results on trace elements and in situ Sr-isotope measurements in crystals and bulk rocks of the 1906–1998 period. It consists of (1) a LP magma reservoir at ~10 km depth, periodically replenished by a mafic magma with relatively low Sr isotope ratios (0.70608) that agrees with the magma ponding zone at ~7.5–11 km depth proposed by *Bertagnini et al.* [2003], (2) an intermediate reservoir at ~3 km depth, which could be a remnant of the old Stromboli struc-

ture according to *Vaggelli et al.* [2003], where LP and HP magmas mix together and continuously crystallize olivine, pyroxene, and plagioclase, (3) an intermediate older crystal-mush body where plagioclase and pyroxene record highly variable and high Sr-isotope signature of the previous magmas, and (4) the uppermost part of the system deduced from the seismic data [*Chouet et al.*, 2003]. During the periodic magma recharge events, LP magma passes through the cumulus reservoir sampling minerals and transporting them into the shallower reservoir. The overall decrease of Sr isotope ratios with time in the HP magmas (1980–1985) was due to the nearly coeval decrease of $^{87}Sr/^{86}Sr$ values in the replenishing LP magmas. This isotopic time variation in the HP magmas (Figure 5c) was used to calculate a short residence time (≈19 ± 12 years) at intermediate level (above reservoir 2) for the magma feeding present-day activity, although this model does not take into account the presence of many xenocrysts having widely variable Sr isotopic ratios [*Francalanci et al.*, 1999, 2004, 2005]. A lower resident time (<520 d) for the HP magmas was calculated by *Gauthier and Condomines* [1999], on the basis of $^{210}Pb/^{226}Ra$ activity ratios, linked to the degassing process in the very shallow magma body (above reservoir 4). The different calculated residence time probably are referred to the different depths of magma rest.

Finally, we show that the large (1930-type eruption) and small-scale (August 1998-type eruption) paroxysmal eruptions can be discriminated on the basis of their mineralogy [*Métrich et al.*, 2001; *Bertagnini et al.*, 2003]. Besides their widespread deposits, the large paroxysms reveal the deep input(s) of volatile-rich, primitive magma batches, weeks or days before the eruption which are identifiable by the presence of high pressure olivine and clinopyroxene (with high Mg/Fe ratios) in the resulting pumices. In contrast, pumices issued from small-scale paroxysms do not have such minerals. They carry xenocrysts showing successive dissolution–crystallization characteristics, whereas crystals in equilibrium with their carrier magma are rare [*Bertagnini et al.*, 2003]. Hence, it has been proposed that the large-scale paroxysms of Stromboli are generated by the rapid uprise, from 7.5 to 11 km, of a fast-moving blob of low-density magmatic foam with no gas/liquid decoupling during its ascent [*Métrich et al.*, 2001; *Bertagnini et al.*, 2003]. The respective role of magma and gas in triggering the paroxysmal eruptions was recently questioned by Allard [2004, 2007] who proposed catastrophic uprise of CO_2-rich gas pockets generated by intermittent gas accumulation in the subvolcanic plumbing system. Accordingly, gas bubbles would be able to carry up primitive melts and crystals in their envelope and bring them rapidly to surface. Whether or not there is gas-accumulation in the plumbing system at a depth of 7.5–11 km is still under debate. The paroxysmal eruption that occurred on April 5, 2003 brought additional data and constraints on the eruption-triggering mechanism.

Acknowledgments. The critical revisions by M.A. Menzies and an anonymous reviewer are greatly acknowledged. Special thanks to P. Pantani for graphic assistance, O. Belhadj for her help in sample preparation, M. Ulivi for helping with isotope analyses in Firenze, and our colleagues for fruitful discussions: A. Aiuppa, P. Allard, M. Burton, P. Papale, M. Pichavant, and B. Scaillet.

REFERENCES

Abbruzzese, D. (1937), Attività dello Stromboli dal 1934 al 1936, *Boll. Vulcanol.*, *2*, 70–76.

Abbruzzese, D., and C. Cavallaro (1956), L'eruzione sottomarina dello Stromboli del 28 febbraio 1955, *Riv. Stromboli*, *4*, 25–29.

Allard, P. (2004), Stromboli, an erupting system powered by steady and catastrophic gas transfer. *INGV workshop: 'L'eruzione di Stromboli (28 Dicembre 2002–20 Luglio 2003), 21–24 May 2004,* Catania, Italy, Abstract, p. 7.

Allard, P. (2007), A CO_2-rich gas trigger of explosive paroxysms at Stromboli volcano (Italy). EGU General Assembly, *Geophys. Res. Abstr.*, *9*, EGU2007-A-08044

Allard, P., J. Carbonnelle, N. Métrich, H. Loyer, and P. Zettwoog (1994), Sulphur output and magma degassing budget of Stromboli volcano, *Nature*, *368*, 326–330.

Armienti, P., L. Francalanci, and P. Landi, (2007), Textural effects of steady state behaviour of the Stromboli feeding system, *J. Volcanol. Geotherm. Res.*, *160*, 86–98.

Arrighi, S., M. Rosi, J.-C. Tanguy, and V. Courtillot (2004), Recent eruptive history of Stromboli (Aeolian Islands, Italy) determined from high-accuracy archeomagnetic dating, *Geophys. Res. Lett.*, *31*, L19603, doi:10.1029/2004GL020627.

Barberi, F., M. Rosi, and A. Sodi (1993), Volcanic hazard assessment at Stromboli based on review of historical data, *Acta Vulcanol*., *3*, 173–187.

Bertagnini, A., M. Coltelli, P. Landi, M. Pompilio, and M. Rosi (1999), Violent explosions yield new insights into dynamics of Stromboli volcano, *Eos Trans. AGU*, *80*(52), 633–636.

Bertagnini A., N. Métrich, P. Landi, and M. Rosi (2003), Stromboli volcano (Aeolian Archipelago, Italy): An open window on the deep-feeding system of a steady state basaltic volcano, *J. Geophys. Res*., *108*(B7), 2336, doi:10.1029/2002JB002146.

Bonaccorso, A., C. Cardaci, M. Coltelli, P. Del Carlo, S. Falsaperla, S. Panucci, M. Pompilio, and L. Villari (1996), Annual report of the world volcanic eruptions in 1993, Stromboli, *Suppl. Bull. Volc. Eruptions*, *35*, 8–14.

Botcharnikov, R., M. Freise, F. Holtz, and H. Berhens (2005), Solubility of C–O–H mixtures in natural melts: New experimental data and application range of recent models. *Ann. Geophys.*, *48*(4–5), 633–646.

Burton, M. R., P. Allard, F. Muré, and A. La Spina (2007a), Magmatic gas composition reveals the source depth of slug-driven Strombolian explosive activity, *Science*, *37*, 227–230.

Burton, M. R., H. M. Mader, and M. Polacci (2007b), The role of gas percolation in quiescent degassing of persistently active basaltic volcanoes, *Earth Planet. Sci. Lett.*, doi:10.1016/j.epsl.2007.08.028.

Calvari, S., M. Pompilio, and D. Andronico (2002), Preliminary report on the eruptive activity occurred at Stromboli volcano on 23 January 2002, *INGV-CT report*, SrvSt20020124. http://www.ct.ingv.it/.

Cavallaro, C. (1957), L'attivita' dello Stromboli dal 1940 al 1953. *Boll. Acc. Gioenia Sci. Nat*. Catania Ser. IV, III, *10*, 526–531.

Cavallaro, C. (1962), L'esplosione dello Stromboli dell'11 luglio 1959. *Riv. Stromboli*, *8*, 11–14.

Chouet, B., G. Saccorotti, P. Dawson, M. Martini, R. Scarpa, G. De Luca, G. Milana, and M. Cattaneo (1999), Broadband measurements of the sources of explosions at Stromboli Volcano, Italy. *Geophys. Res. Lett.*, *26*, 1937–1940.

Clocchiatti, R. (1981), La transition augite–diopside et les liquides silicates intra-cristallins dans les pyroclastes de l'activité actuelle du Stromboli: témoignages de la réinjection et du mélange magmatiques. *Bull. Volcanol.*, *44*, 339–357.

Coltelli, M., S. Falsaperla, P. Del Carlo, M. Pompilio, and A. Bonaccorso (1999), Volcanic, seismic, and ground deformation data concerning the Stromboli volcano in 1995, *Suppl. Bull. Volc. Eruptions*, *35*, 8–14.

Coltelli, M., P. Del Carlo, and M. Pompilio (2000), Vulcano and Stromboli 1. Eruptive activity (Stromboli). *Acta Vulcanol.*, *12*(1–2), 93–95.

De Fino, M, L. La Volpe, S. Falsaperla, G. Frazzetta, G. Neri, L. Francalanci, M. Rosi, and A. Sbrana (1988), The Stromboli eruption of December 6, 1985–April 25, 1986: Volcanological, petrological and seismological data, *Rend. Soc. Ital. Mineral. Petrol*., *43*, 1021–1038.

De Fiore, O. (1915), I fenomeni eruttivi avvenuti allo Stromboli dal 1909 al 1914 ed il loro meccanismo, *Zeit. f. Vulk*., *1*, 225–246.

De Fiore, O. (1923), I fenomeni eruttivi avvenuti allo Stromboli dal 1914 al 1916, *Boll. Soc. Sismol. Ital*., *24*, 9–66.

Di Carlo, I., M. Pichavant, S. Rotolo, and B. Scaillet (2006), Experimental crystallization of a high-K arc basalt: The golden pumice, Stromboli Volcano (Italy), *J. Petrol.*, 1–27, doi:10.1093/petrology/egl011.

Dixon, J. B. (1997), Degassing of alkalic basalts, *Am. Mineral*., *82*, 368–378.

Francalanci, L., M. Barbieri, P. Manetti, A. Peccerillo, and L. Tolomeo (1988), Sr-isotopic systematics in volcanic rocks from the island of Stromboli (Aeolian arc), *Chem. Geol.*, *73*, 164–180.

Francalanci, L., P. Manetti, and A. Peccerillo (1989), Volcanological and magmatological evolution of Stromboli volcano (Aeolian islands): The roles of fractional crystallisation, magma mixing, crustal contamination and source heterogeneity, *Bull. Volcanol*., *51*, 355–378.

Francalanci, L, S. Tommasini, S. Conticelli, and G. R. Davies (1999), Sr isotope evidence for short magma residence time for the 20th century activity at Stromboli volcano, Italy, *Earth Planet. Sci. Lett.*, *167*, 61–69.

Francalanci, L., S. Tommasini, and S. Conticelli (2004), The volcanic activity of Stromboli in the 1906–1998 period: Mineralogical, geochemical and isotope data relevant to the understanding of Strombolian activity, *J. Volcanol. Geotherm. Res.*, *131*, 179–211.

Francalanci, L., G. R. Davies, W. Lustenmhower, S. Tommasini, P. R. D. Mason and S. Conticelli (2005), Old crystal re-cycle and multiple magma reservoirs in the plumbing system of the present day activity at Stromboli volcano, South Italy: Sr-isotope in situ microanalyses, *J. Petrol*., *46,* 1997–2021, doi:10.1093/petrology/egi045.

Gauthier, P. J., and M. Condomines (1999), 210Pb/226Ra radioactive disequilibria in recent lavas and radon degassing: inferences on the magma chamber dynamics at Stromboli and Merapi volcanoes, *Earth Planet. Sci. Lett.*, *172*, 111–126.

Ghiorso, M. S., and R. O. Sack (1995), Chemical transfer in magmatic processes IV, *Contrib. Mineral. Petrol.*, *119*, 197–212.

Global Volcanism Program at http://www.volcano.si.edu/.

Hornig-Kjarsgaard, I., J. Keller, U. Koberski, E. Stadlbauer, L. Francalanci, and R. Lenhart (1993), Geology, stratigraphy and volcanological evolution of the island of Stromboli, Aeolian arc, Italy. *Acta Vulcanol.*, *3*, 21–68.

Istituto Nazionale di Geofisica e Vulcanologia, sezione di Catania at http://www.ct.ingv.it/.

Landi, P., N. Métrich, A. Bertagnini, and M. Rosi (2004), Dynamics of magma mixing and degassing recorded in plagioclase at Stromboli (Aeolian Archipelago, Italy), *Contrib. Mineral. Petrol*., *147*, 213–237.

Landi P., L. Francalanci, M. Pompilio, M. Rosi, R. A. Corsaro, C. M. Petrone, I. Nardini, and L. Miraglia (2006), The December 2002–July 2003 effusive event at Stromboli volcano, Italy: Insights into the shallow plumbing system by petrochemical studies, *J. Volcanol. Geotherm. Res.*, *155*, 263–284.

Lautze, N. C., and B. F. Houghton (2005), Physical mingling of magma and complex eruption dynamics in the shallow conduit at Stromboli volcano, Italy, *Geology*, *33*, 425–428.

Lautze, N. C., and B. F. Houghton (2007), Linking variable explosion style and magma textures during 2002 at Stromboli volcano, Italy, *Bull. Volcanol.*, *69*, 445–460, doi:10.1007/s00445-006-0086-1.

Maramai, A., L. Graziani, and S. Tinti (2005), Tsunamis in the Aeolian Islands (southern Italy): A review, *Mar. Geol.*, *215*, 11–21.

Mercalli, G. (1881), Natura delle eruzioni dello Stromboli ed in generale dell'attività sismo-vulcanica delle Isole Eolie, *Atti Soc. Ital. Sci. Nat.*, *24*, 105–135.

Mercalli, G. (1883), *Vulcani e fenomeni vulcanici in Italia*, 374, A. Forni, Sala Bolognese, Italy.

Mercalli, G. (1884), Notizie sullo stato attuale dei Vulcani attivi italiani, *Atti Soc. Ital. Sci. Nat*., *27*, 184–199.

Mercalli, G. (1907), *I Vulcani Attivi della Terra*, Hoepli, Milan, Italy.

Métrich, N., A. Bertagnini, P. Landi, and M. Rosi (2001), Crystallisation driven by decompression and water loss at Stromboli volcano (Aeolian Islands), *J. Petrol.*, *42*, 1471–1490.

Métrich, N., A. Bertagnini, P. Landi, M. Rosi and O. Belhadj (2005) Triggering mechanism at the origin of paroxysms at Stromboli (Aeolian Archipelago, Italy): The 5 April 2003 eruption, *Geophys. Res. Lett.. 32*, L10305, doi:10.1029/2004GL022257.

Nappi, G. (1976) L'eruzione dello Stromboli del novembre 1975, *Boll. Soc. Geol. It*., *95*, 1975, 991–1008.

Newman, S., and J. B. Lowenstern (2002), VOLATILECALC: A silicate melt–H_2O–CO_2 solution model written in visual basic excel, *Comput. Geosci*., *28*, 597–604.

Papale, P. (1999), Modelling of the solubility of two-component H_2O–CO_2 fluid in silicate liquids, *Am. Mineral*., *84*, 477–492.

Patrick, M, A. J. L. Harris, M. Ripepe, J. Dehn, D. A. Rothery, and S. Calvari (2007), Strombolian explosive styles and source conditions: insights from thermal (FLIR) video, *Bull. Volcanol*., *69*, 769–784, doi:10.1007/s00445-006-0107-0.

Peccerillo, A. and S. R. Taylor (1976), Geochemistry of Eocene calc-alkaline volcanic rocks from the Kastamonu area, Northern Turkey, *Contrib. Mineral. Petrol*., *58*, 63–81.

Perret, F. A. (1916), The lava eruption of Stromboli summer–autumn, 1915, *Am. J. Sci.*, *42*, 436–457.

Petrone, C. M., F. Olmi, E. Braschi, and L. Francalanci (2006), Mineral chemistry profile: A valuable approach to unravel magma mixing processes in the recent volcanic activity of Stromboli, Italy, *Per. Min*., *75*(2–3), 277–292.

Platania, G. (1910), I fenomeni eruttivi dello Stromboli nella primavera del 1907, *Ann. Uff. Cent. Meteor. Geodinam. It*., *30*, 1–27.

Ponte, G. (1919), La catastrofica esplosione dello Stromboli, *R. Accad. Naz. Lincei*, *28*, 89–94.

Ponte, G. (1921), La formidabile esplosione dello Stromboli del 1916, *Mem. R. Com. Geol. It*., *7*, 1–34.

Ponte, G. (1948), Attività straordinaria dello Stromboli, *Ann. Geofis*., *1*, 200–202.

Riccò, A. (1917), Parossismo dello Stromboli del 1915, *Att. Accad. Naz. Lincei*, *25*, 251–259.

Riccò, A., and G. Mercalli (1892), Sopra il periodo eruttivo dello Stromboli cominciato il 24 giugno 1891, *Ann. Uff. Cent. Meteor. Geodinam. It*., *11*, 189–221.

Rittmann, A. (1931), Der Ausbruch des Stromboli am 11 September 1930, *Zeits Vulkanol*., *14*, 47–77.

Rosi, M., A. Bertagnini, and P. Landi (2000), Onset of the persistent activity at Stromboli volcano (Italy), *Bull. Volcanol*., *62*, 294–300.

Speranza, F., M. Pompilio, and L. Sagnotti (2004), Paleomagnetism of spatter lavas from Stromboli volcano (Aeolian Islands, Italy): Implications for the age of paroxysmal eruptions, *Geophys. Res. Lett*., *31*, L02607, doi:10.1029/2003GL018944.

Speranza, F., M. Pompilio, F. D'Ajello Caracciolo, and L. Sagnotti (2008), Holocene eruptive history of the Stromboli volcano: Constraints from paleomagnetic dating, *J. Geophys. Res.*, *113*, B09101, doi:10.1029/2007JB005139.

Vaggelli, G., L. Francalanci, G. Ruggieri, and S. Testi (2003), Persistent polybaric rests of calc-alkaline magmas at Stromboli volcano, Italy: Pressure data from fluid inclusions in restitic quartzite nodules, *Bull. Volcanol*., *65*, 385–404.

Washington, H. S. (1917), Persistence of vents at Stromboli and its bearing on volcanic mechanism, *Bull. Geol. Soc. Am*., *28*, 249–278.

A. Bertagnini, P. Landi, and N. Métrich, Istituto Nazionale di Geofisica e Vulcanologia, Sezione di Pisa, Via della Faggiola 32, 56126 Pisa, Italy. (bertagnini@pi.ingv.it)

S. Conticelli, L. Francalanci, and S. Tommasini, Dipartimento di Scienze della Terra, Università degli Studi di Firenze, Via La Pira 4, 50121 Firenze, Italy.

N. Métrich, Laboratoire Pierre Sue, CNRS-CEA, CE-Saclay, 91191 Gif/Yvette, Italy.